



Published in final edited form as:

*Ann Neurol.* 2018 February ; 83(2): 269–282. doi:10.1002/ana.25144.

## Dysfunctional sarcomere contractility contributes to muscle weakness in *ACTA1*-related nemaline myopathy (NEM3)

B. Joureau<sup>1</sup>, J.M. de Winter<sup>1</sup>, S. Conijn<sup>1</sup>, S.J.P. Bogaards<sup>1</sup>, I. Kovacevic<sup>1</sup>, A. Kalganov<sup>2</sup>, M. Persson<sup>2,3</sup>, J. Lindqvist<sup>4</sup>, G.J.M. Stienen<sup>1</sup>, T.C. Irving<sup>5</sup>, W. Ma<sup>5</sup>, M. Yuen<sup>1,7,8</sup>, N.F. Clarke<sup>7,8</sup>, D.E. Rassier<sup>2</sup>, E. Malfatti<sup>6</sup>, N.B. Romero<sup>6</sup>, A.H. Beggs<sup>9</sup>, and C.A.C Ottenheijm<sup>1,4</sup>

<sup>1</sup>Department of Physiology, VU University Medical Center Amsterdam, The Netherlands

<sup>2</sup>Department of Kinesiology and Physical Education, McGill University, Montreal, Canada

<sup>3</sup>Department of Physiology and Pharmacology, Karolinska Institutet, 171 77 Stockholm, Sweden

<sup>4</sup>Department of Molecular and Cellular Biology and Molecular Cardiovascular Research Program, University of Arizona

<sup>5</sup>The Biophysics Collaborative Access Team (BioCAT), CSRRI and Departments of Biological Sciences, Illinois Institute of Technology, Chicago, IL 60616, USA

<sup>6</sup>Sorbonne Universités, UPMC Univ Paris 06, INSERM UMRS974, CNRS FRE3617, Center for Research in Myology, GH Pitié-Salpêtrière, Paris, France

<sup>7</sup>Institute for Neuroscience and Muscle Research, The Children's Hospital at Westmead, NSW, 2145

<sup>8</sup>Discipline of Pediatrics and Child Health, University of Sydney, Australia

<sup>9</sup>Division of Genetics and Genomics, The Manton Center for Orphan Disease Research, Boston Children's Hospital, Harvard Medical School, Boston, MA, USA

### Abstract

**OBJECTIVE**—Nemaline myopathy (NM) is one of the most common congenital non-dystrophic myopathies and is characterized by muscle weakness, often from birth. Mutations in *ACTA1* are a frequent cause of NM (i.e. NEM3). *ACTA1* encodes alpha-actin 1, the main constituent of the sarcomeric thin filament. The mechanisms by which mutations in *ACTA1* contribute to muscle weakness in NEM3 are incompletely understood. We hypothesized that sarcomeric dysfunction contributes to muscle weakness in NEM3 patients.

**METHODS**—To test this hypothesis, we performed contractility measurements in individual muscle fibers and myofibrils obtained from muscle biopsies of fourteen NEM3 patients with different *ACTA1* mutations. To identify the structural basis for impaired contractility, low angle x-ray diffraction and stimulated emission-depletion microscopy were applied.

---

**Correspondence:** Coen Ottenheijm, PhD, VU University medical center, Department of Physiology, O|2 building, 12W-53, De Boelelaan 1118, 1081 HV Amsterdam, the Netherlands, c.ottenheijm@vumc.nl.

#### AUTHOR CONTRIBUTIONS

Study concept and design: BJ, JMdW, AB, CACO.

Data acquisition and analysis: BJ, JMdW, SC, SB, IK, VK, TI, WM, DR, MP.

Drafting the manuscript and figures: BJ, JMdW, MY, EM, NBR, NFC, GJMS, AHB, DR, TI, AB, CACO.

#### CONFLICTS OF INTEREST

None of the other authors has a financial relationship with a commercial entity that has an interest in the subject of this manuscript.

**RESULTS**—Our findings reveal that muscle fibers of NEM3 patients display a reduced maximal force generating capacity, which is caused by dysfunctional sarcomere contractility in the majority of patients, as revealed by contractility measurements in myofibrils. Low angle x-ray diffraction and stimulated emission-depletion microscopy indicate that dysfunctional sarcomere contractility in NEM3 patients involves a lower number of myosin heads binding to actin during muscle activation. This lower number is not the result of reduced thin filament length. Interestingly, the calcium sensitivity of force is unaffected in some patients, but decreased in others.

**INTERPRETATION**—Thus, dysfunctional sarcomere contractility is an important contributor to muscle weakness in the majority of NEM3 patients, information which is crucial for patient stratification in future clinical trials.

### Keywords

myopathy; skeletal muscle; muscular dystrophy

---

## INTRODUCTION

Nemaline myopathy (NM) is one of the most common congenital non-dystrophic myopathies and is characterized by severe hypotonia, muscle weakness, feeding difficulties, respiratory failure<sup>1</sup>, and the presence of nemaline bodies (rods) in skeletal muscle biopsies<sup>2</sup>. So far, eleven genes have been implicated: alpha-actin 1 (*ACTA1*)<sup>3</sup>, alpha- and beta-tropomyosin (*TPM3* and *TPM2*)<sup>4,5</sup>, nebulin (*NEB*)<sup>6</sup>, leiomodlin-3 (*LMOD3*)<sup>7</sup>, troponin T (*TNNT1*)<sup>8</sup>, cofilin 2 (*CFL2*)<sup>9</sup>, kelch family members 40 (*KLHL40*) and -41 (*KLHL41*)<sup>10,11</sup>, Kelch repeat and BTB (POZ) Domain Containing 13 (*KBTBD13*)<sup>12</sup> and myopalladin (*MYPN*)<sup>13</sup>. In addition, *MYO18B* has been recently identified in one case presenting nemaline myopathy and cardiomyopathy<sup>14</sup> and in two cases with Klippel-Feil syndrome with nemaline myopathy and facial dysmorphism<sup>15</sup>.

*ACTA1*-related NM (NEM3, MIM: 617336) accounts for ~25%<sup>16</sup> of all NM cases and up to 50% of the severe forms<sup>17</sup>. To date, more than 200 pathogenic variants in the *ACTA1* gene have been reported<sup>18</sup>. *ACTA1* encodes globular alpha-actin (~42 kDa), which forms the backbone of muscle thin filaments. The thin filament is a sarcomeric microstructure that is essential for proper muscle contraction: binding of myosin to actin is the molecular basis of force generation by skeletal muscle.

The mechanisms by which mutations in *ACTA1* contribute to contractile weakness in NEM3 patients are incompletely understood. Recent work on muscle biopsies from NEM3 patients indicated that these mechanisms include, depending on the type of mutation, a reduction in length of the thin filament<sup>19</sup> and structural damage to myofibrils<sup>20,21</sup>. It is unknown whether mutations in *ACTA1* affect the contractility of structurally intact sarcomeres. Knowledge on sarcomere contractility in NEM3 patients has therapeutic implications: targeting muscle with structural damage in sarcomeres is cumbersome. On the other hand, sarcomeres that are structurally intact, but dysfunctional, can be targeted with small molecules such as troponin activators<sup>22–24</sup>. Studies on animal models of NEM3 suggest that sarcomere dysfunction contributes to contractile weakness<sup>25–30</sup>, but whether these findings translate to patients

remains unknown. Considering the role of actin in sarcomeric contractility, we hypothesized that sarcomeric dysfunction contributes to contractile weakness in NEM3 patients.

To test this hypothesis, we performed contractility measurements in individual muscle fibers and myofibrils obtained from muscle biopsies from fourteen patients with NEM3. To identify the structural basis for impaired contractility in NEM3 patients, low angle x-ray diffraction and stimulated emission-depletion microscopy were applied. Our findings reveal that sarcomeric dysfunction is an important contributor to contractile weakness in the majority of NEM3 patients.

## MATERIAL AND METHODS

### Muscle biopsies

Biopsies were obtained from the Boston Children's Hospital (NEM3-P1 – NEM3-P4), the Children's Hospital at Westmead (NEM3-P5 – NEM3-P10 and healthy controls [CTRL] 1–4), the Myology Institute in Paris (NEM3-P11 –NEM3-P14), and from Radboud University Medical Center in Nijmegen (CTRL 5 – 7). Table 1 provides clinical and genetic data for the subjects. From all participants, written informed consent was obtained for genetic testing, biobanking, and analysis of muscle biopsies. Biopsies NEM3-P1 –NEM3-P14 were all from genetically confirmed NEM3 patients with clinicopathological diagnoses of NM. CTRL 1–7 are control subjects with no medical history. All biopsies were stored frozen and unfixed at  $-80^{\circ}\text{C}$  until use.

### Muscle fiber contractility

For contractile experiments we isolated single individual fibers or small fiber bundles from muscle biopsies before permeabilization, as described previously<sup>31</sup>. Fiber bundles (cross-sectional area:  $\sim 0.07\text{mm}^2$ , in case of atrophic fibers of patients) and single muscle fibers (control subjects and mildly affected patients) were attached to aluminum clips and mounted between a force transducer (model 403A, Aurora Scientific, Ontario, Canada) and length controller (model 315-CI, Aurora Scientific, Ontario, Canada). We used a setup (model 802D, Aurora Scientific, Ontario, Canada) mounted on top of an inverted microscope (Zeiss Axio Observer A1, Zeiss, Thornwood, NY, USA). Sarcomere length was set using a fast Fourier transform from a region of interest in the real-time camera image and ASI 900B software (Aurora Scientific Inc., Ontario, Canada).

Experiments were performed at sarcomere length  $2.5\ \mu\text{m}$ , a length at which muscle fibers develop maximal force. The width and the depth of the fibers was measured at three points along the fiber with an  $40\times$  objective, and the cross-sectional area (CSA) was calculated assuming an elliptical cross-section. The temperature was kept constant at  $20^{\circ}\text{C}$  using a TEC controller (ASI 825A, Aurora Scientific Inc. Ontario, Canada). Various bathing solutions were used during the experimental protocols: a relaxing solution (100 mM BES; 6.97 mM EGTA; 6.48 mM  $\text{MgCl}_2$ ; 5.89 mM  $\text{Na}_2\text{-ATP}$ ; 40.76 mM K-propionate; 14.5 mM creatine phosphate), a pre-activating solution with low EGTA concentration (pCa 9.0 : 100 mM BES; 0.1 mM EGTA; 6.42 mM  $\text{MgCl}_2$ ; 5.87 mM  $\text{Na}_2\text{-ATP}$ ; 41.14 mM K-propionate; 14.5 mM creatine phosphate; 6.9 mM HDTA), and an activating solution (pCa 4.5 : 100 mM BES; 7.0

mM CaEGTA; 6.28 mM MgCl<sub>2</sub>; 5.97 mM Na<sub>2</sub>-ATP; 40.64 mM K-propionate; 14.5 mM creatine phosphate). The preparations were activated at pCa 4.5 to obtain maximal Ca<sup>2+</sup>-activated force. Maximal active tension was obtained by dividing the force generated at pCa 4.5 by CSA. We studied 6–19 fibers or fiber bundles per biopsy.

Preparations were sequentially transferred from relaxing solution to pre-activating solution and finally activated with solutions with a pCa ranging from 7.0 to 4.5, obtained by appropriate mixing of the relaxing and activating solution. The force-pCa relation obtained was fitted with a Hill equation, providing pCa<sub>50</sub> (pCa giving 50% of maximal active tension) and the Hill coefficient, n<sub>H</sub>, an index of myofilament cooperativity. During measurements at pCa 4.5, the rate of force redevelopment (k<sub>tr</sub>) was measured when a steady force was reached by performing a quick release of 30% of the initial length, which reduced tension to zero. This was followed by a period of unloaded shortening lasting 30 ms. Thereafter, the remaining bound cross-bridges were mechanically detached by rapidly (1ms) re-stretching the preparation back to its original length, after which force redeveloped. Directly after the k<sub>tr</sub> protocol, the active stiffness, defined as the relative proportion of attached and non-attached cross-bridges within an actively contracting fiber, was determined from the change in force upon small amplitude length perturbations (0.3, 0.6 and 0.9% of the fiber length). Stiffness was derived from the slope of the linear regression of the force-length relation. A typical force trace during an experiment is shown in figure 2B.

### Fiber typing

Specialized sodium dodecyl sulfate polyacrylamide gel electrophoresis (SDS-PAGE) was used to determine the myosin heavy chain (MyHC) isoform composition of the muscle fiber preparations studied in the contractility experiments. In short, muscle fibers were denatured by boiling at 80°C for 2 min in SDS sample buffer. The stacking gel contained a 4% acrylamide concentration (pH 6.7), and the separating gel contained 7% acryl-amide (pH 8.7) with 30% glycerol (v/v). The gels were run for 24 h at 15°C and a constant voltage of 275 V. Finally, the gels were silver-stained, scanned, and analyzed with ImageQuant TL (GE Healthcare) software.

### Myofibril contractility

Muscle bundles were dissected from patients and healthy individuals were stored in 50%/50% (v/v) glycerol/rigor solution (50 mM Tris pH 7.0, 100 mM NaCl, 2 mM KCl, 2 mM MgCl<sub>2</sub>, and 10 mM EGTA) containing a cocktail of protease inhibitors (Roche Diagnostics, USA) at –20°C for at least 14 days. On the day of experiments, myofibrils were isolated following procedures previously published. In short, a muscle sample was defrosted in rigor solution at 4°C for ~1 hour. A small piece was cut out and homogenized twice for 5 seconds at 12,000 rpm and twice for 3 seconds at 28,000 rpm (homogenizer VWR Power AHS250, 5 mm generator). This procedure resulted in a solution containing single myofibrils that were transferred into an experimental bath containing relaxing solution (pCa 9.0) and maintained at 15°C. A myofibril was chosen for mechanical measurements based on its striated appearance, and attached between an atomic force cantilever (AFC, ATEC Nanosensors; stiffness 40.27 nN/μm), and a rigid glass micro-needle connected to a piezo motor, which allowed computer-controlled length changes to the myofibrils.

Throughout the experimental procedures, the myofibrils were imaged with an oil immersion 60× magnification microscope objective. The myofibril length, average sarcomere length, and cross-sectional area were measured at the beginning of the experiments. The myofibrils were set to an average sarcomere length of 2.6 μm before activation.

**Myofibril activation and mechanical measurements**—Myofibrils were activated in solutions with pCa ranging from 4.5 to 6.5 with a multi-channel micro-perfusion system attached to a double-barreled pipette<sup>32–34</sup>. When surrounded by a solution containing high Ca<sup>2+</sup> concentration, the myofibrils produced force, causing deflection of the AFC. The deflection of the cantilever was recorded using an optical system<sup>33</sup>, and the force (F) was calculated as  $F = k \cdot d$ , where  $k$  is the cantilever stiffness and  $d$  is the cantilever displacement. Forces were normalized to the myofibril cross-sectional area. The force-pCa relation was fitted to a Hill equation, providing pCa<sub>50</sub> (similarly to analyses performed on single fiber force/pCa data) and the Hill coefficient,  $n_H$ .

During maximal activation, myofibrils were subjected to a rapid shortening protocol (amplitude 30% of sarcomere length; speed 360 μm/sec) during which the force declined and rapidly re-developed to a new steady-state level. We analyzed the rate of force re-development ( $k_{tr}$ ) after this shortening-stretch procedure, which is a measure of the kinetics of myosin molecules shifting from a weakly bound to a strongly bound (force producing) states<sup>35</sup>.  $k_{tr}$  was analyzed with an exponential equation ( $a \cdot \exp(-k^*(t-c)) + b$ ), where  $t$  is time,  $k$  is the rate constant for force re-development,  $a$  is the amplitude of the exponential, and  $b$  and  $c$  are constants.

### Stimulated emission-depletion (STED) microscopy

Fibers were dissected and permeabilized as described above. Immunolabeling was performed as described previously<sup>31</sup>. In brief, fibers were stretched, permeabilized and fixed on a glass slide followed by incubation with Alexa Fluor<sup>®</sup> 488 conjugated Phalloidin (#A12379; Life Technologies) to stain the thin filament. Preparations were then mounted in Mowiol. Super-resolution STED-imaging was performed on a Leica TCS SP8 STED 3× (Leica Microsystems) using an oil immersion objective HCX PL APO STD 100× (numerical aperture 1.4) and a gated Hybrid Detectors. Images were deconvolved using Huygens Professional software (Scientific Volume Imaging). Thin filament length was analyzed by performing line scans along the length of the fiber using ImageJ software (National Institutes of Health, Bethesda, MD). The half of the width at half maximum intensity was used to indicate thin filament length.

### X-ray diffraction studies

Small-angle X-ray diffraction experiments were performed at the BioCAT beamline 18ID (Argonne National Laboratory, Argonne, IL). Fibers were mounted on a custom X-ray diffraction/muscle mechanics setup designed to fit into the X-ray diffraction instrument. Muscle fibers were attached between a high-speed motor (Cambridge model 308B, ~1 ms 90% step response) and a force transducer (Aurora Scientific Model 402A). Sarcomere length was determined using the first-order diffraction band from a He-Ne laser). Sarcomere length was set at 2.5 μm. The small-angle diffraction camera length was ~3m and X-ray

energy was 12 keV. The X-ray exposure times were 1 s with an incident flux of  $\sim 1 \times 10^{12}$  photons/s, and the X-ray diffraction patterns were collected with the use of a Pilatus 3 1M pixel array detector (Dectris Inc.). Images were taken in 100 frame bursts of 10 ms frames separated by 500 ms with the shutter closed to prevent sample heating. In addition, the samples were translated in the beam during the exposures to reduce radiation damage. Separation of the 1,0 equatorial reflections measured from the diffraction pattern were converted to  $d_{1,0}$  lattice spacing via Bragg's law, which can be converted to inter-thick-filament spacing by multiplying  $d_{1,0}$  by  $2/3$ . Fibers were activated remotely by exchanging the solution with pCa 9.0 for a solution with pCa 4.5.

### Statistical Analyses

Data are presented as mean  $\pm$  SEM. GraphPad Prism 7 was used to generate descriptive statistics. For statistical analyses, the Student's t-test was applied.  $P < 0.05$  was considered statistically significant. For the analysis of  $\text{Ca}^{2+}$  sensitivity of force, we used Mann-Whitney U Test to compare each patient to pooled control data, in this case  $P < 0.01$  was considered significant.

## RESULTS

### Patients

Muscle biopsies of fourteen NEM3 patients and of seven control subjects were studied. Table 1 shows the age range of the subjects, the disease severity, and mutation location. Figure 1 displays the location of the mutations in the 3D structure of actin (the molecular model of alpha actin was based on a 2.8 Å atomic structure of rabbit skeletal muscle actin (RCSB Protein Data Bank 1ATN<sup>36</sup>); the ribbon structure showing side chains affected by *ACTA1* assessed in this study was created with Swiss-PDB Viewer v4.1.0<sup>37</sup>). All patients harbored a different mutation in *ACTA1*.

Note that in a previous study<sup>23</sup> we compared the contractility of muscle fibers (i.e., maximal tension and the calcium sensitivity of force; the main parameters of the present study as well) isolated from biopsies of pediatric control subjects with those isolated from biopsies of adult control subjects and found that contractility was comparable. Thus, because of ethical considerations, in the present experiments we studied biopsies of adult controls and compared the findings to those of (mainly) pediatric NEM3 patients.

Furthermore, due to the limited size of the biopsies not all assays could be performed in the biopsies of all fourteen NEM3 patients (per assay the number of studied biopsies is indicated, see below).

### Muscle fiber contractility

**Maximal active tension**—In order to determine whether mutations in *ACTA1* result in abnormal skeletal muscle contraction, we determined the maximal force generating capacity in permeabilized single skeletal muscle fibers and small fiber bundles of all fourteen patients (note that, based on previous work<sup>23</sup>, contractile data from single fibers is comparable to data from small fiber bundles). When assessing the morphology of the fibers used for force



measurements, we noted that they generally displayed well preserved sarcomeric structure, but that fiber diameter was markedly reduced (see Figure 2A). Figure 2B shows a typical force trace of a patient's and a control subject's muscle fiber during exposure to incremental  $\text{Ca}^{2+}$  concentrations. Note that maximal, absolute force was markedly lower in the fiber of the NEM3 patient compared to that in the control subject's fiber. To determine whether the contractile weakness was caused by atrophy, force was normalized to the cross-sectional area of the fiber (i.e. tension). In NEM3 patients, maximal tension of fibers was significantly lower than in fibers of control subjects: tension reduced by ~66%, both fiber types combined; Fig.2C and Table 2. Binning the patients with typical and severe forms of NEM3 and comparing maximal active tension with that in patients with childhood onset/mild forms revealed that patients with mild/childhood onset disease have significantly better contractile function ( $100.4 \pm 14.4$  vs.  $55.4 \pm 11.1$  mN/mm<sup>2</sup>;  $p < 0.01$ ). This suggests that disease severity inversely correlates with fiber contractility. Note that in nine patients only type 1 fiber bundles were isolated from the biopsy, and in one patient both individual type 1 and type 2 fibers. Thus, as type 1 fibers are predominant in NEM3 muscle, we also performed a sub-analysis in which the contractility of type 1 fibers was compared between groups. This analysis showed that the maximal active tension generated by type 1 fibers is reduced by ~49% in NEM3 patients, a reduction that is less pronounced than when fiber types are combined. Thus, muscle fibers of NEM3 patients have a reduced force generating capacity, even after normalizing the force to fiber cross-sectional area. These findings suggest that atrophy alone cannot explain the contractile weakness of muscle fibers in NEM3 patients.

To determine the cause of the lower maximal tension of NEM3 fibers, we studied cross-bridge cycling kinetics (Table 2). First, we measured the rate constant of force re-development ( $k_{tr}$ ) during maximal activation, which provides information regarding the rate of cross-bridge attachment and detachment.  $K_{tr}$  is significantly lower in fibers of NEM3 patients compared to fibers of control subjects. We also determined the stiffness of muscle fibers during maximal activation, which reflects the number of strongly attached cross-bridges. As shown in Figure 2E, active stiffness was lower in fibers of NEM3 patients compared to fibers of control subjects. Finally, we assessed the force generated per cross-bridge by determining the tension/stiffness ratio (Fig. 2F). Fibers of NEM3 patients had a significantly lower tension/stiffness ratio than fibers of control subjects.

These results suggest that the reduced tension in NEM3 patients is caused by a reduced number of force generating cross-bridges and by a reduced force generated per cross-bridge.

To study the  $\text{Ca}^{2+}$  sensitivity of force generation, fibers were exposed to solutions with incremental  $\text{Ca}^{2+}$  concentrations to obtain force-pCa curves, pCa<sub>50</sub> and Hill coefficient (Table 2). When analyzed as a group, there was no shift in the force-pCa relation of NEM3 fibers compared to fibers of control subjects (Fig.2G). However, as shown in Figure 2H, the pCa<sub>50</sub> varied greatly between NEM3 patients, with four patients displaying lower calcium sensitivity of force (i.e. lower pCa<sub>50</sub> than controls; with three of these four mutations being located in subdomain 4 of actin, see Fig.1 for details). Thus, unlike, the maximal force generating capacity, the calcium sensitivity of force of muscle fibers of NEM3 patients is not decreased *per se* but can also be unaltered, depending on the *ACTA1* mutation.

### Low angle X-ray diffraction

The contractility assays in muscle fibers suggest that in fibers of NEM3 patients a lower number of cross-bridges is attached to actin, and that this contributes to the lower maximal tension. To further explore this, we performed low angle x-ray diffraction on muscle fibers of NEM3 patients. Time-resolved x-ray diffraction provides information on structural changes in muscle fibers during fiber activation with nanometer resolution. Due to limited size of the biopsy specimens, these experiments were performed in three NEM3 patients (P4/P5/P9) and in three control subjects. Figure 3A shows a typical equatorial reflection of a NEM3 patient fiber. Analysis of the 1,0 reflection of inactive fibers revealed that thin and thick filament spacing was not different in fibers of NEM3 patients compared to control subjects. Similarly, in inactive fibers the ratio of the 1,1/1,0 intensities, which provides information on the position of the cross-bridges relative to the thin and thick filament, was comparable in NEM3 patients compared to control subjects (Fig.3B). Importantly, the expected increase of the 1,1/1,0 ratio intensities during fiber activation was markedly lower in NEM3 patients compared to the control subjects (Fig.3C). These findings strengthen the notion that fiber activation results in less acto-myosin cross-bridge binding in fibers from NEM3 patients compared to fibers from control subjects. Note that the low sample size precluded statistical testing.

### Myofibril contractility

Next, we aimed to confirm that impaired functioning of sarcomeres contributes to fiber weakness in NEM3 patients by performing contractility assays in single myofibrils. Electron microscopy studies on two NEM3 patients confirmed that muscle fibers of NEM3 patients contain areas of preserved myofibrillar ultrastructure (Fig.4A). Myofibrils (diameter 1–2  $\mu\text{m}$ ) were isolated from eight NEM3 patients and from six control subjects. The myofibrils were attached between a rigid glass needle attached to a length motor and an atomic force cantilever used as force transducer (Fig.4B). Representative force traces of a myofibril from a NEM3 patient and a control subject are shown in Figure 4C. Note the lower force generated by the myofibril of the NEM3 patient. Figure 4D shows that the average maximal tension of myofibrils was reduced by ~50% in the NEM3 patients, and that the maximal tension of myofibrils of six NEM3 patients was lower than that of all control myofibrils. Data on individual subjects are shown in Table 3. Thus, the mechanical studies on both single fibers and single myofibrils show that cross-bridge cycling kinetics are significantly altered in NEM3 patients.

To rule out that the lower contractile strength of NEM3 patient myofibrils was caused by changes in thin filament length or in thin filament number, we measured thin filament length in myofibrils of two NEM3 patients by super-resolution STED microscopy. Analysis of phalloidin line scan intensities (Fig.5A) revealed that thin filament length in these two patients was comparable to thin filament length in control subjects (Figure 5A, right;  $1.21 \pm 0.12 \mu\text{m}$  in NEM3-P2 and  $1.21 \pm 0.06 \mu\text{m}$  in NEM3-P5 vs.  $1.30 \pm 0.01 \mu\text{m}$  in CTRL).



## DISCUSSION

Over the past decades, more than 200 mutations in the *ACTA1* gene have been identified, however, our understanding of the mechanisms by which these mutations contribute to contractile weakness in NM patients has been limited. Through application of muscle fiber and myofibril contractility assays, low angle x-ray diffraction and super-resolution microscopy experiments on muscle biopsies from a large cohort of genetically defined NEM3 patients, the current study shows directly that impaired sarcomeric function contributes to muscle weakness in NEM3. Our data show that one mechanism of this impaired function involves reduced numbers of myosin-based cross-bridges binding to actin during muscle activation. Whether sarcomere dysfunction is exclusive to NEM3 patients or also contributes to muscle weakness in patients with other forms of NM is unknown. Studies on fibers of NEM1, NEM2, NEM4, and NEM10 patients suggest the presence of sarcomere dysfunction<sup>7, 19, 38–43</sup>, but future studies on single myofibrils should provide more conclusive evidence.

### Sarcomere dysfunction in NEM3 patients

NEM3 is caused by mutations in *ACTA1*, which encodes human alpha skeletal actin, a globular molecule (G-actin) consisting of 2 domains (4 subdomains), which are connected by a “hinge” region (ribbon structure shown in light blue, Fig.1). G-actin polymerizes into two twisted strands (F-actin), forming a major structural and functional component of the sarcomeric thin filament. Actin binds to a number of proteins which are crucial for thin filament and sarcomere function, including nebulin, tropomyosin, and myosin. NEM3 is characterized by multiple phenotypes, ranging from late childhood onset with slowly progressive proximal weakness to severe, neonatal onset with facial, respiratory, axial and limb weakness, resulting in early death<sup>44</sup>. Muscle biopsies normally show numerous rods, but also other pathological features have been described<sup>45</sup>. Data on *in vivo* muscle function in NEM3 are scarce. Magnetic resonance imaging of muscles of four NEM3 patients showed that both lower and upper leg muscles (including m. vastus lateralis of which the majority of the studied biopsies were obtained from) had diffuse abnormalities, including fatty replacement of muscle tissue and smaller muscle cross-sectional area<sup>46, 47</sup>. Thus, muscle weakness in NEM3 is at least partly explained by loss of muscle mass. In line with these studies, we observed that isolated muscle fibers of NEM3 patients had smaller cross-sectional area than those of control subjects (Fig.2A; although note that caution is warranted when comparing permeabilized fibers as they swell during treatment with triton-X). It is largely unknown whether the remaining muscle mass has normal function or is dysfunctional and contributes to weakness. Recent work from Malfatti et al. (<sup>21</sup>; manuscript in preparation) showed that muscle fibers of NEM3 patients contain areas of ultrastructural damage. However, this damage could not fully explain the severe muscle fiber weakness in NEM3 patients. As actin is a central component of the sarcomere, the smallest contractile unit in muscle, defects in this protein might have a direct impact on the contractile function of muscle. It is important to establish whether a contractile defect is present as this might direct treatment strategies to improve muscle function<sup>47</sup>. To determine sarcomere contractile function, studies in muscles biopsies are indispensable. To date, these studies are scarce: one study reported that the p.Phe352Ser mutation in *ACTA1* increases contractile function of

human muscle fibers<sup>48</sup>. However, this study was based on only one patient, precluding firm conclusions. A study from our group on biopsies of twelve NEM3 patients reported that a reduction in length of thin filaments contributes to weakness in some, but not all patients<sup>17</sup>. In the present study, we aimed to establish that sarcomere contractile dysfunction contributes to weakness in NEM3 by assessing a large cohort of NEM3 patients. The results show that the maximum force generating capacity of muscle fibers of NEM3 patients is impaired, on average by ~66% (Fig.2), the cause of which includes sarcomere dysfunction, as evidenced by (1) the reduced active stiffness of muscle fibers (Fig.2); (2) the reduced myosin mass transfer from the thick filament backbone towards the actin filament during muscle activation (Fig.3); and (3) impaired contractile force of individual myofibrils (Fig. 4). Note that due to the limited biopsy size, these data are based on six-to-nineteen fiber preparations per biopsy, a number that precludes firm, quantitative conclusions.

This is the first study to determine the contractility of myofibrils from nemaline myopathy patients. It is important to note that if structural damage is present in the myofibrils, they break during the experiment and are excluded from the study. Thus, contribution of ultrastructural damage to the reduced force of myofibrils is highly unlikely (in contrast to the muscle fiber preparations, in which ultrastructural damage contributes to impaired contractile force). Importantly, the reduced force of NEM3 fibers is not *per se* caused by shortened thin filaments. For example, P5 has reduced active stiffness of muscle fibers (Table 1), reduced myosin mass transfer during activation (Fig.3D), reduced myofibril force (Fig.4C), but normal thin filament length as shown by super-resolution microscopy experiments (Fig.5A). Thus, in addition to atrophy and ultrastructural damage in muscle fibers, impaired contractility of sarcomeres contributes to muscle weakness in NEM3.

Importantly, the extent to which these factors contribute to weakness depends on the mutation involved. For instance, fibers of P3 had low active tension, whereas the tension generated by myofibrils was relatively high. This suggests that ultrastructural damage in muscle fibers is an important contributor to weakness in P3. On the other hand, P10 displayed low fiber tension and myofibril tension, suggesting that impaired sarcomere function significantly contributes to muscle weakness in this patient. Consequently, patients with contractile deficits, such as P10, are more likely to benefit from therapy aimed at improving sarcomere contractility than patients, such as P3, whose muscle weakness is mainly caused by structural damage. This information is crucial for patient stratification in future clinical trials.

### **Is the shift towards a higher proportion of type 1 fibers a protective mechanism?**

The majority of biopsies were obtained from the m. vastus lateralis, a muscle that in healthy humans consists of approximately 45% type 1 fibers and 55% type 2 fibers<sup>49</sup>. It is well established that patients with nemaline myopathy can display a predominance of type 1 fibers, a phenomenon that we also observed in the current study (see Table 2; from nine out of fourteen NEM3 patients we isolated mainly/only type 1 fibers). Interestingly, Fig.2C illustrates that from the five biopsies with lowest tension generation, four had a mix of type 1 and type 2 fibers. Indeed, whereas maximal tension in NEM3 patients was decreased by ~66% when all fiber types were compared together, this reduction was ~49% when only type

1 fiber (bundles) were compared. Thus, we postulate that a shift towards a higher proportion of type 1 fibers constitutes a protective mechanism to prevent a dramatic loss of force generating capacity of the overall muscle. In line with this postulation, we reported in previous studies on a nebulin-deficient mouse model a similar shift towards type 1 fibers. Importantly, these type 1 fibers had a relatively preserved contractile force<sup>50</sup>.

### The calcium sensitivity of force

During many daily-life activities, muscles operate at submaximal levels of activity. Thus, whether or not NEM3 affects the force response to submaximal calcium solutions is important to establish. This response, reflected by the  $\text{Ca}^{2+}$ -sensitivity of force, or  $\text{pCa}_{50}$ , was on average comparable between NEM3 patients and controls. However, within the NEM3 cohort, we observed marked variation in the  $\text{Ca}^{2+}$ -sensitivity of force between patients, with lower than normal  $\text{Ca}^{2+}$ -sensitivity in four patients (Fig.2H). A mutation/patient specific effect on  $\text{Ca}^{2+}$ -sensitivity of force has previously been reported for myopathy associated mutations in *ACTA1*<sup>25, 26</sup>, *TPM2* and *TPM3*<sup>38, 51, 52</sup>. When assessing the location of the mutated residues within the actin molecule we found that three of four mutations causing a decreased calcium sensitivity were located in subdomain 4 (see Fig.1 for details). This cluster is not associated with a particular area of known function and given the low number of mutations it is difficult to determine whether a true association between  $\text{Ca}^{2+}$  sensitivity and mutations in this domain exist. Previous studies reported that each actin mutation causes a distinct molecular and histological phenotype, which poorly correlates with the genotype (reviewed in<sup>53</sup>). That we are unable to predict the functional effect of each mutation is likely due to an incomplete understanding of the regulation of actin. Most likely each mutation has a distinct effect on the molecular structure of actin, leading to effects that perhaps change the conformation of the thin filament to favor its ON or OFF state so that different amounts of  $\text{Ca}^{2+}$  are required for force generation. The growing knowledge of actin mutations and their effect on thin filament function, which this study contributes to, will hopefully improve our ability to predict genotype-phenotype correlations in the future.

### Study limitations

First, statistical testing was performed on the NEM3 patients as a group. As each individual NEM3 patient harbored a different mutation in *ACTA1*, which might differentially affect contractility, we considered a single patient to be different from the control subjects if the average of the single patient was more than two standard deviations lower/higher than the average of the controls. This range ( $2 \times \text{SD}$ ) is indicated in Fig. 2C and 2H.

Second, it is unclear whether the muscle tissue in a biopsy specimen is representative for the muscle as whole. Similarly, it is unknown whether fibers isolated from the biopsy represent the quality of all fibers in that biopsy. For instance, in the present study we observed that the contractile force of fibers isolated from P14 depended on the location in the biopsy from which they were obtained: some fibers were of normal size and generated maximal tensions that were nearly comparable to those of control fibers, whereas fibers isolated from another location were very thin and had very low tensions (maximal active tension of the single fibers was  $102.5 \pm 36.9$  vs.  $158.5 \pm 17.1$   $\text{mN/mm}^2$ , slow-twitch vs. fast-twitch, respectively (Table 2;  $n=15$  fibers); maximal active tension of the bundles was  $6.1 \pm 1.3$   $\text{mN/mm}^2$  (bundles

contained a mix of type 1 and type 2 fibers; n=7 bundles). Considering the mild clinical phenotype of this patient (Table 1), we assume that the high tensions of normal appearing fibers better represent the overall quality of the muscle in this patient. Although we observed these discrepant results only in the biopsy of P14, this finding indicates that large variation in fiber quality might be present even within a single biopsy and that caution is warranted when interpreting data from biopsy specimens.

**In conclusion**, this study demonstrates that sarcomere dysfunction contributes to muscle weakness in NEM3 patients. To date, there is no cure for NM, or NEM3 in particular. Each mutation in *ACTA1* results in a particular molecular abnormality, which should be taken into account when considering treatment strategies for NEM3 patients. Recently, we and others<sup>23, 54</sup> have shown that agents that augment the force response to Ca<sup>2+</sup> (eg., levosimendan, and tirasemtiv and its analogues) might benefit patients with muscle weakness, and especially those with reduced Ca<sup>2+</sup>-sensitivity of force generation. Furthermore, interventions aimed at targeting myosin have recently been explored. Intramuscular injections of recombinant adeno-associated viral vectors harboring a myosin transgene improved force production in a NEM3 mouse model<sup>55</sup>. The recent advances made in the development of therapeutic strategies for NEM3 together with a detailed mechanistic understanding of weakness in NM will one day result in development of clinically effective therapies to improve the quality of life of NM patients.

## Acknowledgments

The authors thank Elizabeth DeChene for assistance ascertaining and enrolling NEM3 patients and managing collection of muscle biopsies for analysis, and Dr. Pankaj Agrawal for genotyping. This work was supported in part by National Institutes of Health grants from the National Institute of Child Health and Human Development (R01 HD075802), National Institute of Arthritis and Musculoskeletal and Skin Diseases (R01 AR044345), Muscular Dystrophy Association (USA) grant MDA383249, the Dutch Foundation for Scientific Research (NWO-VIDI; 016.126.319) and by generous support from the AUism Family Foundation and A Foundation Building Strength for Nemaline Myopathy. M.Y. was supported by a University of Sydney Australian Postgraduate Award and an International Postgraduate Research Scholarship. This work was supported by the National Health and Medical Research Council of Australia [APP571287 and APP1022707 to N.F.C.; APP1121651 to M.Y.]. M.P. was funded by a postdoctoral grant from the Swedish Research Council (grant # 2015-00385). The research used resources of the Advanced Photon Source, a U.S. Department of Energy (DOE) Office of Science User Facility operated for the DOE Office of Science by Argonne National Laboratory under Contract No. DE-AC02-06CH11357. This project was supported by grant 9 P41 GM103622 from the National Institute of General Medical Sciences of the National Institutes of Health. We thank dr. Sandra Cooper and Leigh Waddell (Institute for Neuroscience and Muscle Research, Kid's Research Institute, Children's Hospital at Westmead, Sydney) for making available muscle biopsies. The content is solely the responsibility of the authors and does not necessarily reflect the official views of the National Institute of General Medical Sciences or the National Institutes of Health.

## BIBLIOGRAPHY

1. Schnell C, Kan A, North KN. 'An artefact gone awry': identification of the first case of nemaline myopathy by Dr R.D.K. Reye. *Neuromuscul Disord.* 2000 Jun; 10(4-5):307-12. [PubMed: 10838259]
2. Malfatti E, Romero NB. Nemaline myopathies: State of the art. *Rev Neurol (Paris).* 2016 Oct; 172(10):614-9. [PubMed: 27659899]
3. Nowak KJ, Wattanasirichaigoon D, Goebel HH, et al. Mutations in the skeletal muscle alpha-actin gene in patients with actin myopathy and nemaline myopathy. *Nature Genetics.* 1999 Oct; 23(2): 208-12. [PubMed: 10508519]

4. Laing NG, Wilton SD, Akkari PA, et al. A mutation in the alpha tropomyosin gene TPM3 associated with autosomal dominant nemaline myopathy NEM1. *Nat Genet.* 1995 Jun;10(2):249. [PubMed: 7663526]
5. Donner K, Ollikainen M, Ridanpaa M, et al. Mutations in the beta-tropomyosin (TPM2) gene--a rare cause of nemaline myopathy. *Neuromuscul Disord.* 2002 Feb; 12(2):151–8. [PubMed: 11738357]
6. Pelin K, Hilpela P, Donner K, et al. Mutations in the nebulin gene associated with autosomal recessive nemaline myopathy. *Proc Natl Acad Sci U S A.* 1999 Mar; 96(5):2305–10. [PubMed: 10051637]
7. Yuen M, Sandaradura SA, Dowling JJ, et al. Leiomodlin-3 dysfunction results in thin filament disorganization and nemaline myopathy. *The Journal of Clinical Investigation.* 2014 Nov; 124(11):4693–708. [PubMed: 25250574]
8. Johnston JJ, Kelley RI, Crawford TO, et al. A novel nemaline myopathy in the Amish caused by a mutation in troponin T1. *Am J Hum Genet.* 2000 Oct; 67(4):814–21. [PubMed: 10952871]
9. Thirion C, Stucka R, Mendel B, et al. Characterization of human muscle type cofilin (CFL2) in normal and regenerating muscle. *Eur J Biochem.* 2001 Jun; 268(12):3473–82. [PubMed: 11422377]
10. Ravenscroft G, Miyatake S, Lehtokari V-L, et al. Mutations in KLHL40 are a frequent cause of severe autosomal-recessive nemaline myopathy. *American Journal of Human Genetics.* 2013 Jul; 93(1):6–18. [PubMed: 23746549]
11. Gupta VA, Ravenscroft G, Shaheen R, et al. Identification of KLHL41 Mutations Implicates BTB-Kelch-Mediated Ubiquitination as an Alternate Pathway to Myofibrillar Disruption in Nemaline Myopathy. *American journal of human genetics.* 2013 Dec; 93(6):1108–17. [PubMed: 24268659]
12. Sambuughin N, Yau KS, Olivé M, et al. Dominant mutations in KBTBD13, a member of the BTB/Kelch family, cause nemaline myopathy with cores. *American Journal of Human Genetics.* 2010 Dec; 87(6):842–7. [PubMed: 21109227]
13. Miyatake S, Mitsuhashi S, Hayashi YK, et al. Biallelic Mutations in MYPN, Encoding Myopalladin, Are Associated with Childhood-Onset, Slowly Progressive Nemaline Myopathy. *Am J Hum Genet.* 2017 Jan; 100(1):169–78. [PubMed: 28017374]
14. Malfatti E, Bohm J, Lacène E, Romero N, Laporte J. A premature stop codon in MYO18B is associated with severe nemaline myopathy with cardiomyopathy. *Journal of Neuromuscular Diseases.* 2015 Sep; 2(3):219–27. [PubMed: 27858739]
15. Alazami AM, Kentab AY, Faqeih E, et al. A novel syndrome of Klippel-Feil anomaly, myopathy, and characteristic facies is linked to a null mutation in MYO18B. *J Med Genet.* 2015 Jun; 52(6):400–4. [PubMed: 25748484]
16. Romero NB, Sandaradura SA, Clarke NF. Recent advances in nemaline myopathy. *Current opinion in neurology.* 2013 Oct; 26(5):519–26. [PubMed: 23995272]
17. Agrawal PB, Strickland CD, Midgett C, et al. Heterogeneity of nemaline myopathy cases with skeletal muscle alpha-actin gene mutations. *Ann Neurol.* 2004 Jul; 56(1):86–96. [PubMed: 15236405]
18. Nowak KJ, Ravenscroft G, Laing NG. Skeletal muscle alpha-actin diseases (actinopathies): pathology and mechanisms. *Acta Neuropathol.* 2013 Jan; 125(1):19–32. [PubMed: 22825594]
19. de Winter JM, Joureau B, Lee EJ, et al. Mutation-Specific Effects on Thin Filament Length in Thin Filament Myopathy. *Ann Neurol.* 2016 Jun; 79(6):959–69. [PubMed: 27074222]
20. Malfatti E, Lehtokari VL, Böhm J, et al. Muscle histopathology in nebulin-related nemaline myopathy: ultrastructural findings correlated to disease severity and genotype. *Acta Neuropathol Commun.* 2014 Apr;2:44. [PubMed: 24725366]
21. Malfatti E, Monges S, Lornage X, et al. ACTA1-related nemaline myopathy: Reappraisal of the histopathological findings. *Neuromuscul Disord.* 2016 Oct;26(Supplement 2):S133.
22. Russell AJ, Hartman JJ, Hinken AC, et al. Activation of fast skeletal muscle troponin as a potential therapeutic approach for treating neuromuscular diseases. *Nature medicine.* 2012 Feb; 18(3):452–5.
23. de Winter JM, Buck D, Hidalgo C, et al. Troponin activator augments muscle force in nemaline myopathy patients with nebulin mutations. *J Med Genet.* 2013 Jun; 50(6):383–92. [PubMed: 23572184]

24. Hooijman PE, Beishuizen A, Witt CC, et al. Diaphragm muscle fiber weakness and ubiquitin-proteasome activation in critically ill patients. *Am J Respir Crit Care Med.* 2015 May; 191(10): 1126–38. [PubMed: 25760684]
25. Gineste C, Duhamel G, Le Fur Y, et al. Multimodal MRI and (31)P-MRS investigations of the ACTA1(Asp286Gly) mouse model of nemaline myopathy provide evidence of impaired in vivo muscle function, altered muscle structure and disturbed energy metabolism. *PLoS One.* 2013; 8(8):e72294. [PubMed: 23977274]
26. Gineste C, Le Fur Y, Vilmen C, et al. Combined MRI and (31)P-MRS investigations of the ACTA1(H40Y) mouse model of nemaline myopathy show impaired muscle function and altered energy metabolism. *PLoS One.* 2013; 8(4):e61517. [PubMed: 23613869]
27. Ochala J, Ravenscroft G, Laing NG, Nowak KJ. Nemaline myopathy-related skeletal muscle alpha-actin (ACTA1) mutation, Asp286Gly, prevents proper strong myosin binding and triggers muscle weakness. *PLoS One.* 2012; 7(9):e45923. [PubMed: 23029319]
28. Ravenscroft G, Jackaman C, Bringans S, et al. Mouse models of dominant ACTA1 disease recapitulate human disease and provide insight into therapies. *Brain.* 2011 Apr; 134(Pt 4):1101–15. [PubMed: 21303860]
29. Ravenscroft G, Jackaman C, Sewry CA, et al. Actin nemaline myopathy mouse reproduces disease, suggests other actin disease phenotypes and provides cautionary note on muscle transgene expression. *PLoS One.* 2011; 6(12):e28699. [PubMed: 22174871]
30. Lindqvist J, Cheng AJ, Renaud G, Hardeman EC, Ochala J. Distinct underlying mechanisms of limb and respiratory muscle fiber weaknesses in nemaline myopathy. *Journal of neuropathology and experimental neurology.* 2013 Jun; 72(6):472–81. [PubMed: 23656990]
31. Ottenheijm CAC, Buck D, Winter JMd, et al. Deleting exon 55 from the nebulin gene induces severe muscle weakness in a mouse model for nemaline myopathy. *Brain.* 2013 May; 136(Pt 6): 1718–31. [PubMed: 23715096]
32. Ribeiro PA, Ribeiro JP, Minozzo FC, et al. Contractility of myofibrils from the heart and diaphragm muscles measured with atomic force cantilevers: effects of heart-specific deletion of arginyl-tRNA-protein transferase. *Int J Cardiol.* 2013 Oct; 168(4):3564–71. [PubMed: 23739549]
33. Labuda A, Brastaviceanu T, Pavlov I, Paul W, Rassier DE. Optical detection system for probing cantilever deflections parallel to a sample surface. *Rev Sci Instrum.* 2011 Jan; 82(1):013701. [PubMed: 21280831]
34. Rassier DE. Pre-power stroke cross bridges contribute to force during stretch of skeletal muscle myofibrils. *Proc Biol Sci.* 2008 Nov; 275(1651):2577–86. [PubMed: 18664437]
35. Brenner B, Eisenberg E. Rate of force generation in muscle: correlation with actomyosin ATPase activity in solution. *Proceedings of the National Academy of Sciences of the United States of America.* 1986 May; 83(10):3542–6. [PubMed: 2939452]
36. Kabsch W, Mannherz HG, Suck D, Pai EF, Holmes KC. Atomic structure of the actin:DNase I complex. *Nature.* 1990 Sep; 347(6288):37–44. [PubMed: 2395459]
37. Guex N, Peitsch MC. Swiss-Model and the Swiss-PdbViewer: an environment for comparative protein modeling. *Electrophoresis.* 1997 Dec; 18(15):2714–23. [PubMed: 9504803]
38. Mokbel N, Ilkovski B, Kreissl M, et al. K7del is a common TPM2 gene mutation associated with nemaline myopathy and raised myofibre calcium sensitivity. *Brain.* 2013 Feb; 136(Pt 2):494–507. [PubMed: 23378224]
39. Ottenheijm CAC, Witt CC, Stienen GJ, Labeit S, Beggs AH, Granzier H. Thin filament length dysregulation contributes to muscle weakness in nemaline myopathy patients with nebulin deficiency. *Human molecular genetics.* 2009 Jul; 18(13):2359–69. [PubMed: 19346529]
40. Ottenheijm CAC, Hooijman P, DeChene ET, Stienen GJ, Beggs AH, Granzier H. Altered myofilament function depresses force generation in patients with nebulin-based nemaline myopathy (NEM2). *Journal of Structural Biology.* 2010 May; 170(2):334–43. [PubMed: 19944167]
41. Ottenheijm CAC, Lawlor MW, Stienen GJM, Granzier H, Beggs AH. Changes in cross-bridge cycling underlie muscle weakness in patients with tropomyosin 3-based myopathy. *Human molecular genetics.* 2011 May; 20(10):2015–25. [PubMed: 21357678]



42. Ochala J, Lehtokari VL, Iwamoto H, et al. Disrupted myosin cross-bridge cycling kinetics triggers muscle weakness in nebulin-related myopathy. *Faseb J*. 2011 Jun; 25(6):1903–13. [PubMed: 21350120]
43. Ochala J, Gokhin DS, Penisson-Besnier I, et al. Congenital myopathy-causing tropomyosin mutations induce thin filament dysfunction via distinct physiological mechanisms. *Hum Mol Genet*. 2012 Oct; 21(20):4473–85. [PubMed: 22798622]
44. Wallgren-Petersson C, Pelin K, Nowak KJ, et al. Genotype-phenotype correlations in nemaline myopathy caused by mutations in the genes for nebulin and skeletal muscle alpha-actin. *Neuromuscul Disord*. 2004 Sep; 14(8–9):461–70. [PubMed: 15336686]
45. Sewry CA, Wallgren-Petersson C. Myopathology in congenital myopathies. *Neuropathol Appl Neurobiol*. 2017 Feb; 43(1):5–23.
46. Quijano-Roy S, Carlier RY, Fischer D. Muscle imaging in congenital myopathies. *Semin Pediatr Neurol*. 2011 Dec; 18(4):221–9. [PubMed: 22172417]
47. Jungbluth H, Sewry CA, Counsell S, et al. Magnetic resonance imaging of muscle in nemaline myopathy. *Neuromuscul Disord*. 2004 Dec; 14(12):779–84. [PubMed: 15564032]
48. Lindqvist J, Penisson-Besnier I, Iwamoto H, Li M, Yagi N, Ochala J. A myopathy-related actin mutation increases contractile function. *Acta Neuropathol*. 2012 May; 123(5):739–46. [PubMed: 22358459]
49. Johnson MA, Polgar J, Weightman D, Appleton D. Data on the distribution of fibre types in thirty-six human muscles. An autopsy study. *J Neurol Sci*. 1973 Jan; 18(1):111–29. [PubMed: 4120482]
50. Li F, Buck D, De Winter J, et al. Nebulin deficiency in adult muscle causes sarcomere defects and muscle-type-dependent changes in trophicity: novel insights in nemaline myopathy. *Hum Mol Genet*. 2015 Sep; 24(18):5219–33. [PubMed: 26123491]
51. Yuen M, Cooper ST, Marston SB, et al. Muscle weakness in TPM3-myopathy is due to reduced Ca<sup>2+</sup>-sensitivity and impaired acto-myosin cross-bridge cycling in slow fibres. *Hum Mol Genet*. 2015 Nov; 24(22):6278–92. [PubMed: 26307083]
52. Donkervoort S, Papadaki M, de Winter JM, et al. TPM3 deletions cause a hypercontractile congenital muscle stiffness phenotype. *Ann Neurol*. 2015 Dec; 78(6):982–94. [PubMed: 26418456]
53. Feng JJ, Marston S. Genotype-phenotype correlations in ACTA1 mutations that cause congenital myopathies. *Neuromuscul Disord*. 2009 Jan; 19(1):6–16. [PubMed: 18976909]
54. de Winter JM, Joureau B, Sequeira V, et al. Effect of levosimendan on the contractility of muscle fibers from nemaline myopathy patients with mutations in the nebulin gene. *Skeletal Muscle*. 2015 Apr; 5:12. [PubMed: 25949787]
55. Lindqvist J, Levy Y, Pati-Alam A, Hardeman EC, Gregorevic P, Ochala J. Modulating myosin restores muscle function in a mouse model of nemaline myopathy. *Ann Neurol*. 2016 May; 79(5):717–25.
56. Li XE, Tobacman LS, Mun JY, Craig R, Fischer S, Lehman W. Tropomyosin position on F-actin revealed by EM reconstruction and computational chemistry. *Biophys J*. 2011 Feb; 100(4):1005–13. [PubMed: 21320445]
57. Laing NG, Dye DE, Wallgren-Petersson C, et al. Mutations and Polymorphisms of the Skeletal Muscle  $\alpha$ -Actin Gene (ACTA1). *Hum Mutat*. 2009 Sep; 30(9):1267–77. 58. [PubMed: 19562689]
58. Ilkovski B, Cooper ST, Nowak K, et al. Nemaline myopathy caused by mutations in the muscle alpha-skeletal-actin gene. *American Journal of Human Genetics*. 2001; 68(6):1333–43. 2001/06//. [PubMed: 11333380]
59. Hutchinson DO, Charlton A, Laing NG, Ilkovski B, North KN. Autosomal dominant nemaline myopathy with intranuclear rods due to mutation of the skeletal muscle ACTA1 gene: clinical and pathological variability within a kindred. *Neuromuscul Disord*. 2006 Feb; 16(2):113–21. [PubMed: 16427282]
60. Sparrow JC, Nowak KJ, Durling HJ, et al. Muscle disease caused by mutations in the skeletal muscle alpha-actin gene (ACTA1). *Neuromuscular disorders: NMD*. 2003; 13(7–8):519–31. 2003/09//. [PubMed: 12921789]

61. Nowak KJ, Wattanasirichaigoon D, Goebel HH, et al. Mutations in the skeletal muscle alpha-actin gene in patients with actin myopathy and nemaline myopathy. *Nature Genetics*. 1999 Oct; 23(2): 208–12. [PubMed: 10508519]

Author Manuscript

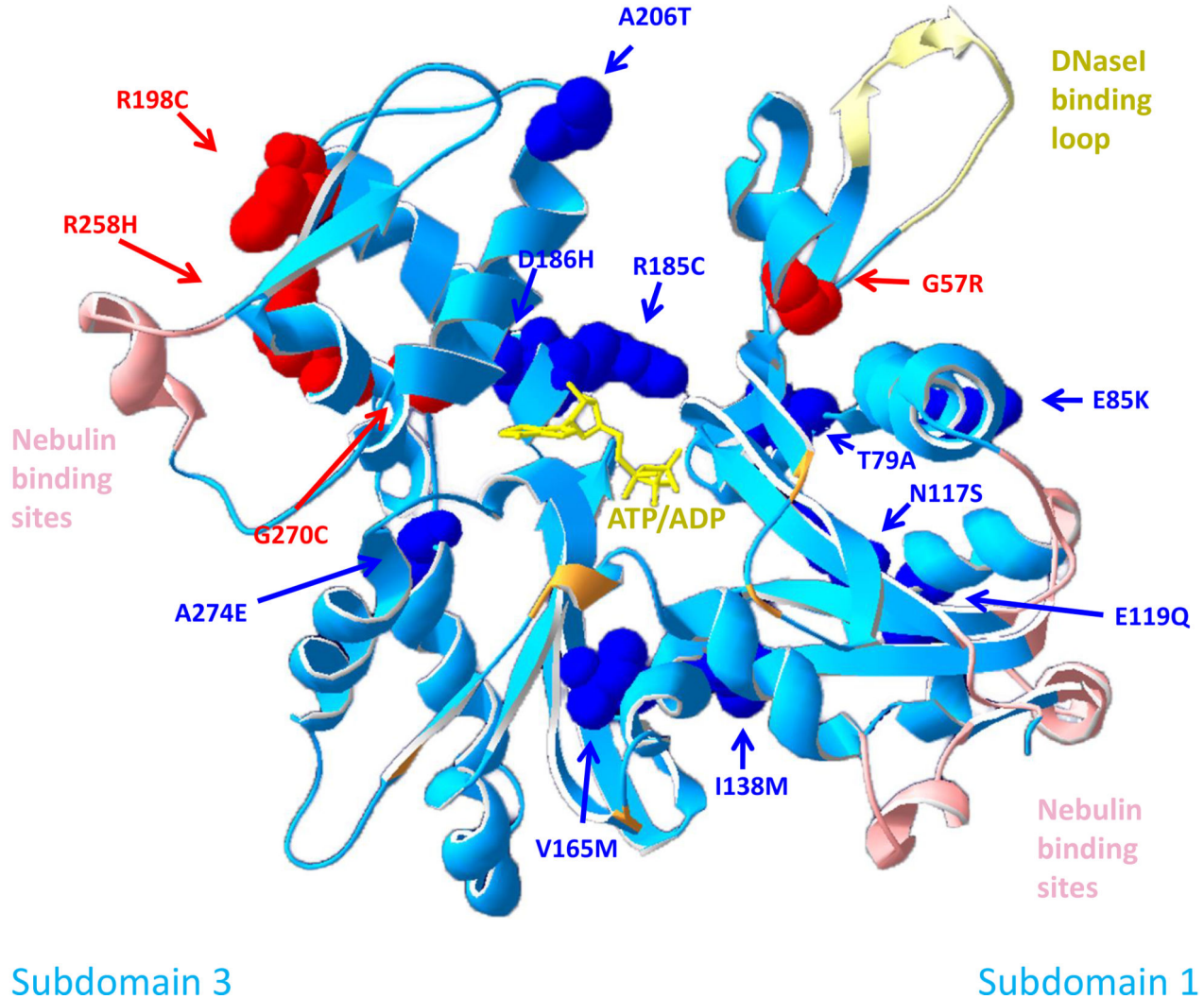
Author Manuscript

Author Manuscript

Author Manuscript

Subdomain 4

Subdomain 2

**Figure 1.**

Molecular model of an actin monomer highlighting the position of mutated residues analyzed in this study (the molecular model of alpha actin was based on a 2.8 Å atomic structure of rabbit skeletal muscle actin (RCSB Protein Data Bank 1ATN,<sup>36</sup>). The ribbon structure showing side chains affected by *ACTA1* assessed in this study was created with Swiss-PDB Viewer v4.1.0<sup>37</sup>). Human alpha skeletal actin is a globular molecule consisting of 2 domains (4 subdomains) which are connected by a “hinge” region (ribbon structure shown in light blue). A cleft is located between the two domains containing a divalent cation and ATP/ADP (yellow). Actin polymerizes into two twisted strands where each actin molecule interacts with four neighboring monomers. The DNase1 binding loop (pale yellow) is involved in actin-actin binding by forming a lock-in-key interaction between neighboring actin molecules. Details on further residues involved in actin-actin interactions can be found in<sup>53</sup>. Actin binds to a number of proteins which are crucial for its function. Important

binding partners include nebulin (amino acids involved in binding are 98–103, 127–132, 361–368, 228–238, 4–8, 350–358, shown in light pink<sup>53</sup>), tropomyosin (Asp27, Arg30, Arg149, Lys328, Lys329, Lys330, Pro335 and Glu336,<sup>56</sup> shown in orange) and myosin (via amino acid 2–6, 26–27, 101–102, 146, 334, 335, 343, 351, 354<sup>53</sup>). The 14 actin residues affected by the mutations we investigated in this study are highlighted in red and blue depending on their effect on the Ca<sup>2+</sup> sensitivity of force generation (red = reduced Ca<sup>2+</sup> sensitivity; dark blue = Ca<sup>2+</sup> sensitivity comparable to controls). Three of four residues reducing Ca<sup>2+</sup> sensitivity are located within subdomain 4.

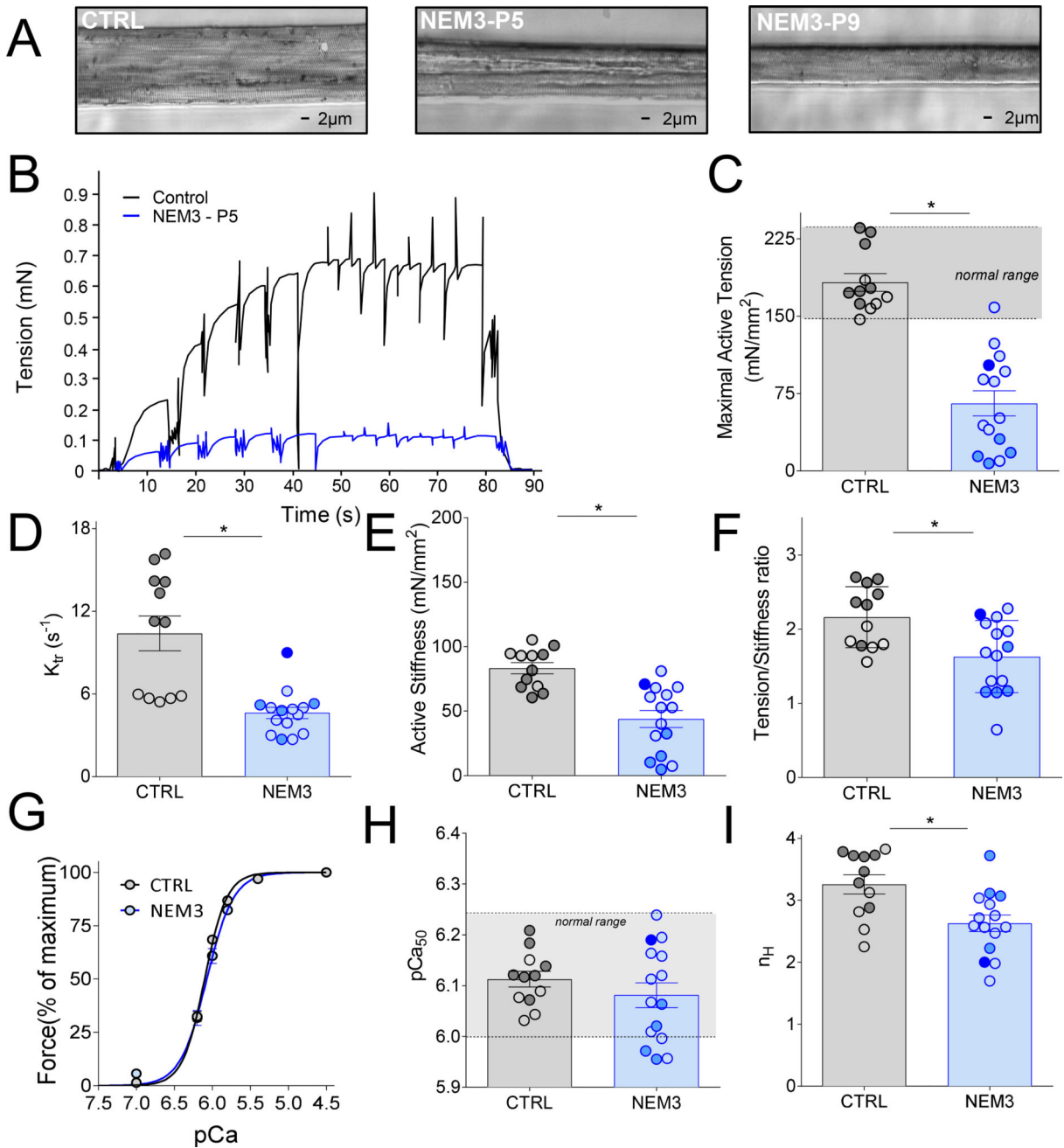


**Figure 2.** (A) Typical example of a permeabilized muscle fiber preparation of a control subject (left) and of two NEM3 patients (middle and right) mounted in the contractility setup. (B) Typical tracing showing the force response to incremental Ca<sup>2+</sup> concentrations followed by the measurement of the rate constant redevelopment ( $k_{tr}$ ) and the active stiffness in a control and a NEM3 patient (P5); (C) Maximal active tension (force normalized to CSA),  $k_{tr}$  (D), active stiffness (E), and the tension stiffness ratio (F) were significantly lower in NEM3 patients than in control subjects; (G) Force-pCa relationship showing the average of all controls (n=7) and all NEM3 patients (n=14), showing no difference in mean calcium sensitivity

between the groups. However, analyzing individual patients illustrated that some patients have increased and some decreased  $pCa_{50}(H)$ ; 'normal range': mean of controls  $\pm 2*SD$ . The Hill coefficient,  $n_H(I)$ , was significantly decreased compared to control subjects. Note: slow-twitch fibers in light color, fast-twitch fibers in dark color, bundle of mixed fiber-types in intermediate color (only in NEM3 patients).



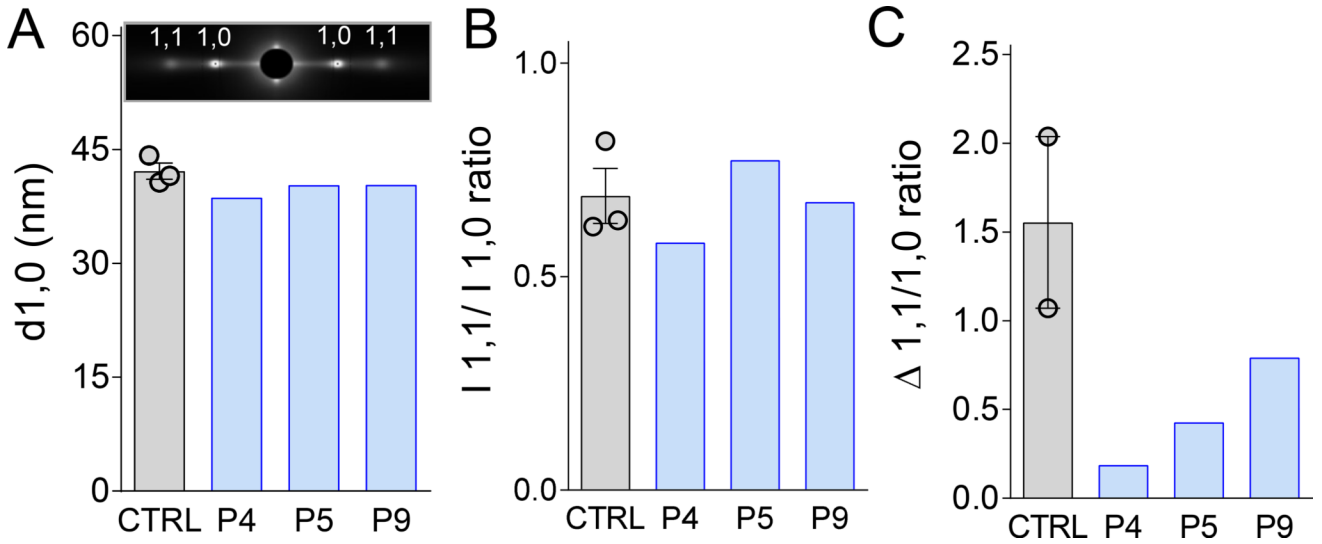


**Figure 3.** (A, top) Typical equatorial reflection obtained from a fiber preparation of a NEM3 patient (P4). (A, bottom) The separation of the 1,0 equatorial reflections (which reflects thin-thick filament lattice spacing) is comparable between fibers of control subjects (n=3) and NEM3 patients (NEM3-P5, n=4) in an inactive state. (B) In an inactive state, the I<sub>1,1</sub>/I<sub>1,0</sub> intensity ratio, reflecting the position of myosin-based cross-bridges relative to actin, was also not different between NEM3 patients and control subjects; (C) During activation, the expected increase in the I<sub>1,1</sub>/I<sub>1,0</sub> intensity ratio was reduced in the NEM3 patients compared to control subjects.

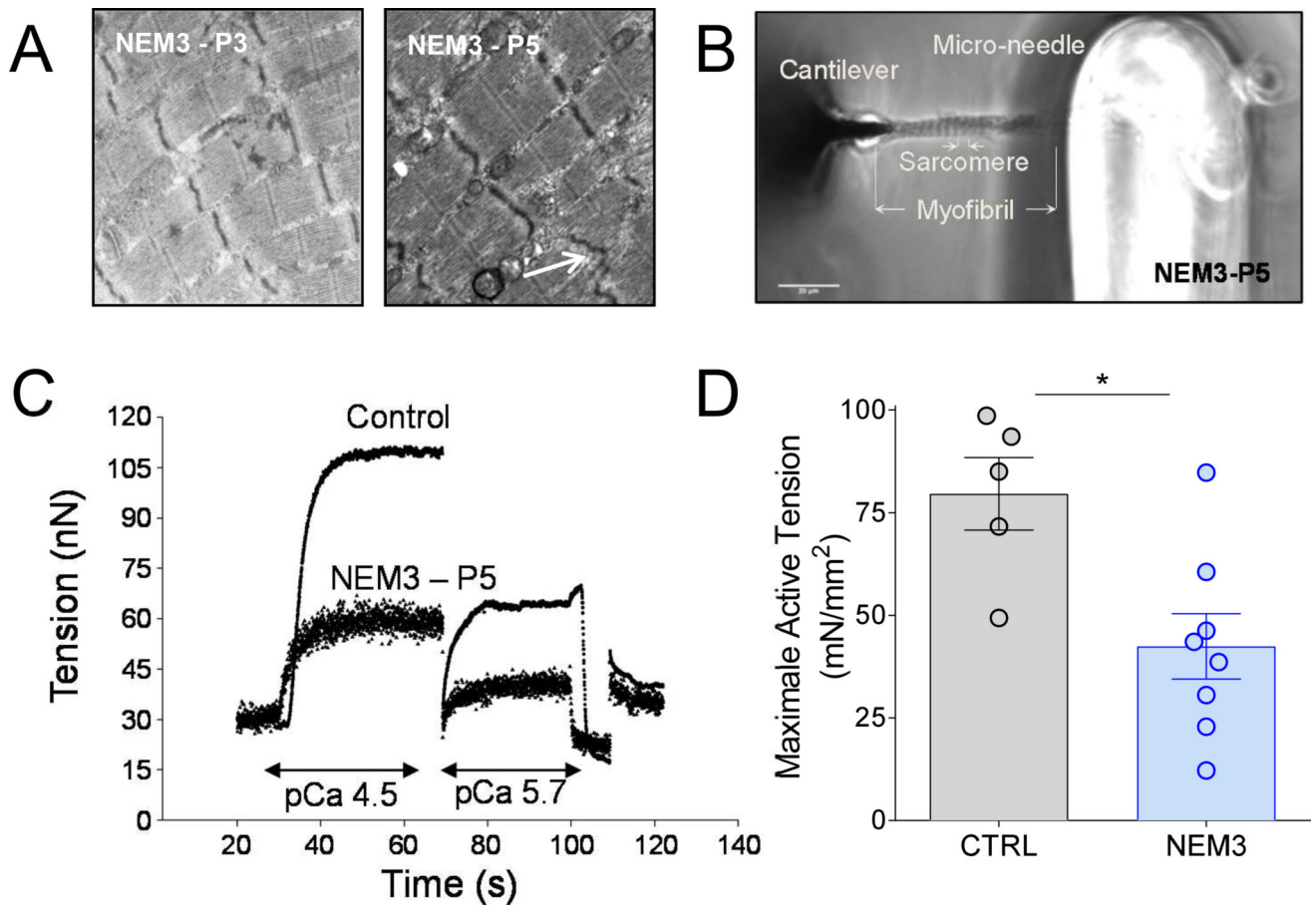


**Figure 4.** Electron microscopy images of muscle fibers of two NEM3 patients, presenting areas of preserved myofibrillar structure, but also mild Z-line irregularities (B, indicated by an arrow). (B) Photograph of a myofibril (NEM3-P5) mounted between a microneedle and a cantilever to measure its contractility; (C) Typical force trace showing that the force generating capacity of a myofibril of a NEM3 patient (P5) at different  $\text{Ca}^{2+}$  concentrations (pCa 4.5 and 5.7) and of a control subject; (D) Maximal active tension is lower in NEM3 patients compared to control subjects.

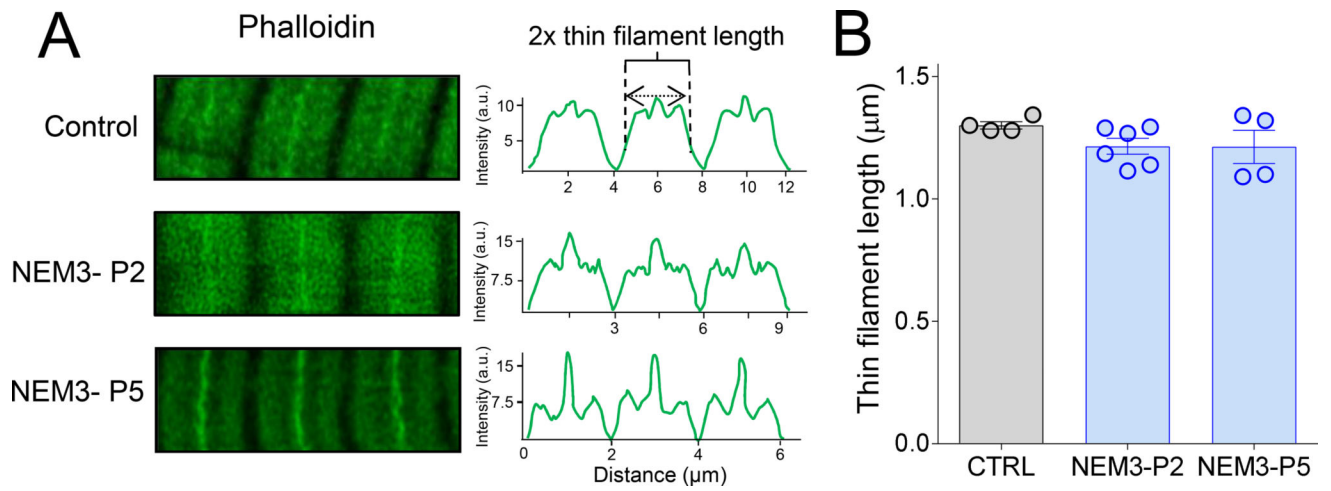


**Figure 5.**  
 (A) Super-resolution (STED) microscopy on myofibrils from control subjects and NEM3 patients. Thin filaments were stained with phalloidin-AlexaFluor 488. (B). Thin filament length was comparable between four control subjects and two NEM3 patients.

**Table 1**

Clinical and genetic information on subjects.

Patient ID	Mutations	Age	Patient ID	Disease	Clinical Severity	References
<b>Control (CTRL)</b>						
CTRL - 1	N/A	21 yrs	-	-	-	51
CTRL - 2	N/A	31 yrs	-	-	-	51
CTRL - 3	N/A	54 yrs	-	-	-	51
CTRL - 4	N/A	39 yrs	-	-	-	51
CTRL - 5	N/A	53 yrs	-	-	-	U
CTRL - 6	N/A	51 yrs	-	-	-	U
CTRL - 7	N/A	51 yrs	-	-	-	U
<b>Skeletal muscle alpha-actin patients (NEM3)</b>						
NEM3 - P1	p. Gly57Arg	7 mo	BOS922-1   T866	NM	Typical	19
NEM3 - P2	p. Arg258His	2 mo	BOS927-1   T865	NM	Typical	19
NEM3 - P3	p. Thr79Ala	10 mo	BOS95-1   T77	NM	Typical	57
NEM3 - P4	p. Glu85Lys	2.8 yrs	BOS349-1   T256	NM	Typical	57
NEM3 - P5	p. Ala274Gly	3 yrs	-	NM	Typical	57
NEM3 - P6	p. Ala206Thr	60 yrs	-	NM	Mild	4
NEM3 - P7	p. Gly270Cys	4 yrs	-	NM	Childhood onset	58
NEM3 - P8	p. Val165Met	65 yrs	-	NM	Mild	59
NEM3 - P9	p. Asn117Ser	17 yrs	-	NM	Childhood onset	58
NEM3 - P10	p. Asp186His	1 mo	-	NM	Severe	2
NEM3 - P11	p. Arg198Cys	5 yrs	-	NM	Severe	U
NEM3 - P12	p. Ile138Met	23 yrs	-	NM	Typical	60
NEM3 - P13	p. Glu119Gln	1 yr	-	NM	Severe	U
NEM3 - P14	p. Arg185Cys	41 yrs	-	NM	Mild	61

U: unpublished

**Table 2**

Functional data of single fibers of NEM3 patients and controls.

Patients ID	Maximal Active Tension(mN/mm <sup>2</sup> )		K <sub>tr</sub> (s <sup>-1</sup> )		Active Stiffness (mN/mm <sup>2</sup> )		Force per cross bridge		pCa50		nH	
	Slow	Fast	Slow	Fast	Slow	Fast	Slow	Fast	Slow	Fast		
<b>Control (CTRL)</b>												
CTRL - 1	162.0±5.1	162	5.7±0.2	16.2	92.9±4.7	60.6	1.8±0.1	2.7	6.09±0.01	6.12	3.8±0.9	3.7
CTRL - 2	146.8±19.7	174.1±10.9	5.8	11.3±1.2	69.2	68.7±5.4	1.8	2.6±0.1	6.03±0.02	6.07±0.02	2.8±0.1	3.7±0.3
CTRL - 3	168.6±7.4	172.5±16.3	6.0±0.2	13.3±1.6	94.7±4.4	74.8±11.0	1.8±0.2	2.4±0.2	6.08±0.01	6.12±0.04	3.1±0.5	3.5±0.2
CTRL - 4	-	177.2±15.6	-	11.2±0.9	-	63.7±11.4	-	3.2±0.4	-	6.12±0.02	-	3.3±0.2
CTRL - 5	184.8±18.2	220.1±3.5	5.4±0.4	14.2±1.7	93.0±12.4	81.5±1	2.0±0.1	2.7±0.01	6.15±0.03	6.21±0.03	2.2±0.2	3.8±0.2
CTRL - 6	157.3±2.7	231.6±6.5	5.9±0.1	15.8±1.1	105.3±13.6	93.8±1.5	1.6±0.2	2.5±0.1	6.04±0.02	6.14±0.03	2.5±0.3	3.7±0.1
CTRL - 7	-	235.4±25	-	14.1±0.7	-	100.9±9.7	-	2.3±0.05	-	6.18±0.02	-	2.9±0.1
<b>Mean</b>	<b>163.9±6.3</b>	<b>196.1±11.9</b>	<b>5.7±0.1</b>	<b>13.7±0.7</b>	<b>91.0±5.9</b>	<b>77.7±5.8</b>	<b>1.8±0.1</b>	<b>2.4±0.1</b>	<b>6.08±0.02</b>	<b>6.14±0.02</b>	<b>2.9±0.3</b>	<b>3.5±0.1</b>
<b>Skeletal muscle alpha-actin patients (NEM3)</b>												
NEM3 - P1	44.0±5.2 <sup>(1000)</sup>		3.9±0.4		30.9±4.8		1.6±0.2		6.01±0.01		2.9±0.2	
NEM3 - P2	17.7±2.0 <sup>(50/50)</sup>		5.2±0.3		10.3±1.5		1.8±0.1		5.97±0.02		2.2±0.2	
NEM3 - P3	30.9±6.5 <sup>(89/41)</sup>		5.3±0.6		32.5±16.7		1.2±0.4		6.06±0.08		3.1±1.2	
NEM3 - P4	96.4±15 <sup>#</sup>		5.0±0.6		60.9±16.7		2.0±0.2		6.20±0.04		2.0±0.2	
NEM3 - P5	88.7±14.4 <sup>(1000)</sup>		4.1±0.4		52.8±13.0		2.3±0.7		6.24±0.04		2.6±0.3	
NEM3 - P6	123.3±5.5 <sup>#</sup>		5.0±0.2		52.8±3.0		2.2±0.01		6.16±0.01		2.6±0.1	
NEM3 - P7	51.1±6.8 <sup>(1000)</sup>		3.1±0.5		40.1±4.5		1.3±0.1		5.96±0.03		2.7±0.2	
NEM3 - P8	111.2±8.2 <sup>#</sup>		6.2±1.0		68.0±4.8		2.1±0.1		6.07±0.02		2.6±0.1	
NEM3 - P9	86.7±18.1 <sup>#</sup>		4.5±0.3		68.6±17.0		1.9±0.1		6.11±0.04		2.8±0.2	
NEM3 - P10	9.7±1.6 <sup>(1000)</sup>		3.0±0.5		7.4±0.5		1.7±0.1		6.00±0.07		2.5±0.4	
NEM3 - P11	7.4±2.0 <sup>(84/16)</sup>		2.7±0.6		4.8±1.2		1.1±0.2		5.96±0.02		3.1±0.4	
NEM3 - P12	40.1±12 <sup>(1000/0)</sup>		2.7±0.8		62.6±14.6		0.6±0.2		6.16±0.09		3.0±0.5	
NEM3 - P13	14.0±3.4 <sup>(33/67)</sup>		4.8±0.8		15.0±5.6		1.2±0.3		6.02±0.04		3.7±1.0	
NEM3 - P14	102.5±36.9	158.5±17.1	4.9±0.5	9.0±1.1	81±20.1	70.8±6.3	1.3±0.1	2.21±0.9	6.12±0.03	6.19±0.03	1.7±0.5	2.9±0.2

Patients ID	Maximal Active Tension(miN/mm <sup>2</sup> )	K <sub>r</sub> (s <sup>-1</sup> )	Active Stiffness (miN/mm <sup>2</sup> )	Force per cross bridge	pCa50	n <sub>H</sub>
Mean	60.8±11.3*	4.5±0.3*	45.3±8.5*	1.6±0.1*	6.08±0.02	2.7±0.1*

# : individual type 1 fibers obtained from biopsy, no type 2 fibers obtained;

(x/x') : fiber bundles obtained from biopsy, x/x (slow/fast) indicates fiber type composition in the bundles as determined by SDS-PAGE. Note that from P14 individual type 1 (left) and type 2 (right) fibers were isolated from the biopsy, and both data points are shown in Fig.2C.

\* : Significantly different from CTRL (P < 0.05). Data are mean±SEM.



**Table 3**

Functional data of myofibrils from NEM3 patients and controls.

Patient ID	Maximal Active Tension (nN/ $\mu\text{m}^2$ )	$K_{tr}(s^{-1})$	pCa <sub>50</sub>	n <sub>H</sub>
<b>Control (CTRL)</b>				
CTRL - 1	98.6±7.0	8.8±0.4	5.7±0.1	2.3±0.3
CTRL - 2	49.4±14.9	4.6±0.5	5.8±0.1	1.5±0.3
CTRL - 3	63.9±21.2	6.4±0.4	6.0±0.2	1.1±0.004
CTRL - 5	93.5±12.7	5.3±0.7	6.1±0.1	3.7±1.1
CTRL - 6	71.6±6.6	5.0±1.0	5.9±0.1	1.9±0.01
<b>Mean</b>	<b>79.6±9.5</b>	<b>6.0±0.6</b>	<b>5.9±0.1</b>	<b>2.1±0.3</b>
<b>Skeletal muscle alpha-actin patients (NEM3)</b>				
NEM3 - P1	22.8±2.5	2.6±0.4	5.4±0.1	1.1±0.1
NEM3 - P2	38.8±0.6	3.5±0.3	5.9±0.1	1.4±0.2
NEM3 - P3	60.6±6.1	3.3±0.3	5.8±0.1	1.3±0.1
NEM3 - P4	43.5±4.6	1.8±0.2	5.7±0.1	1.4±0.1
NEM3 - P5	46.2±1.5	0.3±0.1	5.7±0.02	1.5±0.1
NEM3 - P6	84.8±5.1	0.5±0.2	5.8±0.1	1.5±0.1
NEM3 - P9	30.6±2.9	4.5±0.2	5.7±0.05	1.1±0.1
NEM3 - P10	12.2±6.1	2.5±0.5	5.7±0.1	2.1±0.2
<b>Mean</b>	<b>42.4±8.0*</b>	<b>2.4±0.3*</b>	<b>5.7±0.05</b>	<b>1.4±0.1</b>

Data are mean±SEM.